IET Renewable Power Generation

Research Article

IET Journals
The Institution of Engineering and Technology

Power management in PV-battery-hydro based standalone microgrid

ISSN 1752-1416
Received on 21st August 2017
Revised 30th October 2017
Accepted on 26th November 2017
E-First on 21st December 2017
doi: 10.1049/iet-rpg.2017.0566
www.ietdl.org

Seema Kewat[1] ✉, *Bhim Singh*[2,3], *Ikhlaq Hussain*[3]

[1]*Indian Institute of Technology, Delhi, India*
[2]*Indian Institute of Technology, Electrical Engineering, Delhi, India*
[3]*Department of Electrical Engineering, IIT Delhi, Delhi, India*
✉ *E-mail: seemajmi2013@gmail.com*

Abstract: This work deals with the frequency regulation, voltage regulation, power management and load levelling of solar photovoltaic (PV)-battery-hydro based microgrid (MG). In this MG, the battery capacity is reduced as compared to a system, where the battery is directly connected to the DC bus of the voltage source converter (VSC). A bidirectional DC–DC converter connects the battery to the DC bus and it controls the charging and discharging current of the battery. It also regulates the DC bus voltage of VSC, frequency and voltage of MG. The proposed system manages the power flow of different sources like hydro and solar PV array. However, the load levelling is managed through the battery. The battery with VSC absorbs the sudden load changes, resulting in rapid regulation of DC link voltage, frequency and voltage of MG. Therefore, the system voltage and frequency regulation allows the active power balance along with the auxiliary services such as reactive power support, source current harmonics mitigation and voltage harmonics reduction at the point of common interconnection. The experimental results under various steady state and dynamic conditions, exhibit the excellent performance of the proposed system and validate the design and control of proposed MG.

Nomenclature

v_{sab}, v_{sbc}, v_{sca}	sensed line voltage at point of common interconnection (PCI)
V_{tm}*, V_{tm}, V_{er}	reference PCI voltage amplitude, sensed PCI voltage amplitude and their error
i_{La}, i_{Lb}, i_{Lc}	load currents of phase 'a', 'b' and 'c'
i_{sa}, i_{sb}, i_{sc}	sensed source currents of phase 'a', 'b' and 'c'
i_{sa}*, i_{sb}*, i_{sc}*	reference source currents of phase 'a', 'b' and 'c'
V_{pv}, I_{pv}	solar PV voltage and current
V_{dc}*, V_{dc}, V_{dcer}	reference DC-link voltage, DC-link voltage of VSC and their error
I_b*, I_b, I_{ber}	reference battery current, sensed battery current and their error
C_{dc}, L_f, R_f, C_f	DC-link capacitor, coupling inductor, resistance and capacitor of ripple filter
L_b, L_{dc}	boost converter inductor, BDDC inductor

1 Introduction

In the present scenario, the proliferation of energy demand of households and industries, create challenges and set a limit on the power generation from the conventional energy sources [1]. The solution to this problem lies somewhere in the core of power generation through renewable energy sources (RES) [2], with efficient, cost effective and reliable generation through RES. The rural electrification is provided by a standalone diesel generator and an integration of other RES in [3–7]. However, the setback for this technology is an RES intermittent nature. This leads to the component over sizing while designing any hybrid renewable energy based microgrid (MG). This also increases the initial cost, operational cost, and life cycle cost. These shortcomings open the window for hybridisation of RES to back up each other. However, this requires the optimal integration of RES and various types of hybrid systems. Philip *et al.* [8] have demonstrated the diesel engine driven generator, battery and photovoltaic (PV) array based hybrid standalone MG. Due to increasing fuel prices and increased pollution concerns, the diesel PV based MG has limited scope. Moreover, the topology presented in the literature has the battery directly connected to the direct current (DC) link. Due to this, the battery is exposed to direct DC link voltage fluctuations. This reduces the battery life. In the proposed topology, the battery is connected to the DC-link through a bidirectional DC–DC converter (BDDC). Hence second harmonic current is eliminated from the battery current. Grid connected RES are another class of topologies, which are available in the literature [9]. These topologies based MGs are possible at those places, where grid availability is easy. However, the proposed topology is also possible in rural areas. Merabet *et al.* [10] and Prakash *et al.* [11] have reported the wind, PV and battery based MG. They have established the control algorithm to look after the power compatibility and power management among different RES in the MG. Wind and PV both being of intermittent nature, present a problem to the optimal sizing [12] of the energy storage. The minimum required battery size, depends on the critical load that the MG must be capable of feeding when both the solar and wind, are unavailable. In this way, the storage may be oversized. However, in the proposed MG, hydro also supports the critical load, thus the battery size is reduced. Moreover, initial and operational costs, are low and maintenance requirement is also less. The small hydro power plant in remote regions is recognised as a promising energy source to generate electricity. The small hydro system up to 100 kW rating does not require governor control based turbine prime mover and curtails down the cost of the turbine. The generator used in the small hydro has many variations [13–16]. Synchronous generator [13], permanent magnet synchronous generator [14], synchronous reluctance generator and self-excited induction generator (SEIG) [15, 16], are some of them. However, the most cost effective, efficient, rugged, and easy to use generator in the small hydro system is SEIG. Additionally, the maintenance requirement is also less as compared with its synchronous counterpart. Moreover, SEIG has the drawback that it demands reactive power or magnetising current for producing the desired terminal voltage. Therefore, an excitation capacitor bank provides magnetising current for regulating the terminal voltage of the generator [17–19]. The hydro-based generating system operates in almost constant power mode so that if the load changes, the frequency, and voltage also changes from their reference values.

Therefore, voltage and frequency in the standalone SEIG based hydro system are maintained with the help of an electronic load controller.

However, in the case of light load, the dump load is needed to dissipate the extra power for regulating the frequency and voltage. Though the use of a dump load, serves the purpose of voltage and frequency regulation, however, it increases the cost of the system and dissipates useful energy in the form of heat. In contrast, the battery energy storage (BES) based controller for frequency and voltage eliminates the dump load through the power management of the different energy sources as discussed in [20–22]. Serban *et al.* [22] have described the system controller for maintaining frequency and voltage of the system and BES is used for supplying surplus power at peak load condition. In this topology, BES is used for supplying surplus power at peak load condition. However, in this topology, BES is used in floating mode and the battery charging and discharging are not controlled, which makes the system costly and the battery life is decreased. Therefore, a battery control is necessary for effective utilisation of the battery. Mostly, a BDDC controls the charging and discharging current of the battery as discussed in [23]. Eghtedarpour *et al*. [23] have discussed distributed charging and discharging control of the battery. However, the designed controller lacks in managing the power and fulfilling the power demand, when the power demand is more than the maximum deliverable power of the BES. Due to this, the DC-link voltage continuously falls from its minimum DC-link voltage. However, in this proposed system, the controller is designed in such a way that it maintains the DC link voltage even when the required power is more than the maximum deliverable power of the battery. Since the controller also takes the PV power in consideration to supply the demand and to maintain the DC link voltage. Moreover, the BES with voltage source converter (VSC) also improves the power quality of the system, manages the load unbalance, and fulfils the peak load demand [24]. Seema *et al*. [25] have discussed only simulation-based analysis of a PV-battery-hydro MG with controlled battery. The BDDC is used to control the DC bus voltage with controlled battery current.

In this system, PV-battery-hydro based MG is designed for low voltage, which supplies power to small pockets of customers. The proposed MG consists of two energy sources namely hydro and PV with BES. The hydro-based MG adds stiffness and inertia to the system voltage and also increases the reliability of the MG as compared with the wind based MG. An integration of BES eliminates the need for a dump load and adds to the functionality of the MG. This BES is controlled by a bidirectional converter, which reduces the capacity of storage and utilises the battery effectively. Moreover, BES maintains the continuity of the supply in varying load conditions. The generation of stable, maximum and continuous energy from the PV array is achieved through incremental conductance (INC) maximum power point tracking (MPPT) technique [26]. Additionally, some ancillary services are achieved like current harmonics mitigation, voltage harmonics reduction and reactive power support at the point of common interconnection (PCI). The VSC switching is based on the synchronous reference frame (SRF) theory. Therefore, the proposed standalone PV hydro based MG is highly suitable to serve the remote places where electrification is either not yet done or the cost of the electrification is costly. The proposed MG has the following distinctive features:

(i) In the proposed MG, the hydro generator runs at almost constant power, therefore, the sudden load change causes the frequency and generated a voltage at PCI to vary. One way of regulating the voltage and frequency is by controlling the water inlet to the hydro through the mechanical controller. However, due to the mechanical devices involved, the dynamic response of the controller is not very fast. Therefore, the mechanical speed regulator is not suitable for sudden changing loads. Therefore, in this proposed MG, the storage battery with VSC, is used to regulate the frequency of the system.
(ii) During the period of a load change, the controller estimates the load power demand and total generated power. If the load demand is more than the generated power, the controller draws the remaining power from the battery to balance the power demand. Similarly, for light load condition, the battery takes the extra power to maintain the frequency of the system.
(iii) The proposed MG is also suitable to feed the non-linear load and the harmonic currents required by the non-linear load are supplied by the VSC. Therefore, the hydro generator does not supply the harmonic currents and voltage at PCI is of good quality.
(iv) The proposed MG mitigates the negative impacts of solar PV array caused by the intermittent nature of the solar irradiance. Due to this intermittency, the power generated by the solar PV array changes continuously. Therefore, the storage battery absorbs power fluctuations and maintains the frequency of the MG.
(v) In the proposed MG, the battery is connected to the DC link of the VSC through BDDC, rather than connecting the battery directly at DC link. The advantage of not connecting the battery directly at DC-link reduces the voltage rating of the battery. Moreover, the battery is not directly exposed to the DC link ripple mostly dominant second harmonic. In this proposed topology, the filter of the BDDC smoothens the charging current, thereby, increasing the battery life.

2 Structure and design of proposed MG

The proposed MG consists of two RES namely hydro, solar PV array along with a BES, a boost converter for MPPT operation and a BDDC for the battery control, as shown in Fig. 1*a*. A SEIG is used as a hydro generator, which is driven by an unregulated turbine operating in the constant power region. A VSC is connected to the PCI through the coupling inductors. The battery shares the common DC bus of the VSC through the BDDC and solar PV system is also connected to the DC bus of the VSC through the boost converter. Moreover, the ripple filter, linear and non-linear loads are connected to the PCI. The hardware implementation of the proposed MG is done using the digital processor (dSPACE-1103). The inputs of the digital processor are PCI voltages, load currents, source currents, battery current, sensed DC bus voltage, solar PV voltage, and current. However, these parameters are sensed using the Hall-effect voltage and current sensors. After this, the digital processor reads these sensed data via analog to digital converter (ADC) and processes according to the SRF based control algorithm and generates the switching pulses for the VSC.

2.1 Design of PV boost converter

The solar PV array is made of modules, which are connected in series and parallel. In an experimental prototype, a solar PV array rating is considered as 2.48 kW. The solar PV maximum power is extracted in two stages. The first stage is to harness the maximum available from the solar PV array using a boost converter and the second stage is to deliver the maximum harnessed power to the load and the battery. The input voltage of a boost converter is the maximum power point (MPP) voltage of the PV array, which is considered as 307 V. The inductor (L_b) of the boost converter is designed for a duty cycle estimated as

$$D = (V_{dc} - V_{pv})/V_{dc} = (360 - 307)/360 = 0.147. \quad (1)$$

The designed value of a boost inductor is given as [8]

$$L_b = \frac{V_{mp} \times D}{\Delta i_{rp} \times f_s} = \frac{307 \times 0.15}{0.1 \times 8 \times 20 \times 10^3} = 2.87\,\text{mH} \cong 3\,\text{mH}, \quad (2)$$

where ripple current is equal to 10% of the solar PV current at MPP and f_S is switching frequency, which is considered as 20 kHz.

2.2 Design of DC bus capacitor and coupling inductors of VSC

The minimum DC bus voltage for power transfer should be at least equal to 1.1 times the peak of line voltage, i.e. $V_{dc} = 1.1 \times V_{sab} \times \sqrt{2} = 230 \times \sqrt{2} \times 1.1 = 358$ V. Therefore, a DC bus

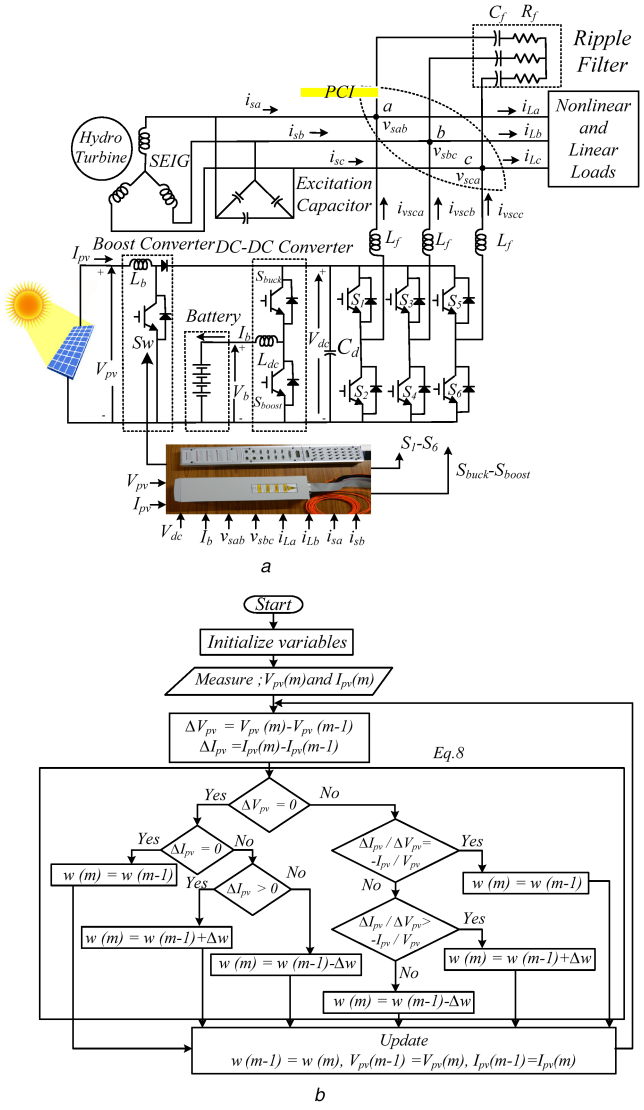

Fig. 1 *Microgrid Topology and MPPT Control*
(a) Proposed PV-battery-hydro MG, ***(b)*** INC based MPP algorithm

capacitor is calculated for DC bus voltage of 360 V and it is given as

$$C_{\mathrm{d}} = \frac{P_{\mathrm{dc}}/V_{\mathrm{dc}}}{2\times\omega\times\Delta V_{\mathrm{dc}}} = \frac{2485/360}{2\times 314\times 0.015\times 360} = 2854.61\,\mu\mathrm{F} \cong 3000\,\mu\mathrm{F}. \quad (3)$$

The interfacing inductor is designed for elimination of high-frequency switching harmonics from the VSC current. The coupling inductor is designed as [18]

$$L_{\mathrm{f}} = \frac{m\times V_{\mathrm{dc}}}{6\times f_{\mathrm{s}}\times h\times\Delta i_{\mathrm{c}}} = \frac{360}{6\times 10\times 10^{3}\times 1.2\times 11\times 0.10} = 4.5\ \mathrm{mH} \cong 5\ \mathrm{mH}. \quad (4)$$

where f_{s} is the switching frequency and it is considered as 10 kHz. Δi_{c} is the ripple current and it is considered as 10% of fundamental supply current. m and h are the constant values, which are considered as 1 and 1.2, respectively.

2.3 Design of bidirectional converter

The bidirectional DC–DC inductor (BDDC), which connects the battery to the DC bus, is designed to operate as a buck converter while charging the battery and operates as a boost converter in the battery discharging mode. This inductor of the BES is designed as,

For buck mode operation of the bidirectional converter, filter inductor of the battery is designed as duty cycle $(D) = V_{\mathrm{b}}/V_{\mathrm{dc}} = 240/360 = 0.66$, and an inductor, L_{dc} is as

$$L_{\mathrm{dc}} = \frac{D(V_{\mathrm{dc}}-V_{\mathrm{b}})}{f_{\mathrm{s}}\Delta I_{\mathrm{L}}} = \frac{0.66\times(360-240)}{20\times 10^{3}\times 5\times 0.2} = 3.96\ \mathrm{mH} \cong 4\ \mathrm{mH}, \quad (5)$$

where V_{b} is the battery voltage and it is 240 V, V_{dc} is the DC-link voltage and it is considered as 360 V. ΔI_{L} is the ripple current and it is considered as 20% of charging current. f_{s} is the switching frequency and its value is 20 kHz.

For boost mode operation of bidirectional converter, the filter inductor of the battery is designed as duty cycle $(D) = (V_{\mathrm{dc}} - V_{\mathrm{b}})/V_{\mathrm{b}} = (360-240)/360 = 0.33$

$$L_{\mathrm{dc}} = \frac{V_{\mathrm{b}}D}{f_{\mathrm{s}}\Delta I_{\mathrm{L}}} = \frac{0.33\times 240}{20\times 10^{3}\times 5\times 0.2} = 3.96\ \mathrm{mH} \cong 4\ \mathrm{mH}, \quad (6)$$

where V_{dc} is the DC link voltage and it is 360 V. V_{b} is the battery voltage and it is 240 V. ΔI_{L} is the ripple current and it is considered as 20% of discharging current. Therefore, the filter inductor of the BES is considered as 4 mH.

2.4 Design of battery and ripple filter

Based on the total capacity of the hydro and solar PV array, the energy storage system capacity is selected. In case, the load is isolated from the MG, the battery should be able to take the whole generated power of the hydro and solar PV array. Moreover, in this extreme operating condition, the battery should regulate the frequency and voltage of the MG. Hence, the battery rating is selected as 240 V, 14 Ah. The ripple filter is designed to suppress the high-frequency noise caused by the switching the VSC. The ripple filter is a low pass filter and it is the series combination of the capacitor and resistance and their values, are selected as 10 μF and 5 Ω. The other parameters of the MG are given in the Appendix.

3 Control strategy

The details of the control algorithm are given here, which are used for maintaining frequency and voltage of the system. Here, an INC-MPPT technique harnesses the maximum power from the solar PV array and the battery is controlled by a bidirectional controller.

3.1 INC-based MPP strategy

The proposed MG consists of two renewable energy systems one is hydro and another one is solar PV system as shown in Fig. 1*a*. The maximum power of the solar PV array is extracted in two stages. One stage is the MPP algorithm, which estimates the duty cycle of a boost converter for achieving maximum power. The second stage is the VSC, which delivers a maximum power of the PV system to the battery and the load. The INC-based MPP technique is used for harnessing the maximum power from the PV system as shown in Fig. 1*b*. The maximum available power is given as

$$P_{\mathrm{mpp}} = V_{\mathrm{pv}}\times I_{\mathrm{pv}}. \quad (7)$$

The MPP point is achieved at that point where the PV power derivative with respect to the PV voltage is equal to zero. The governed equations of INC algorithm is given as

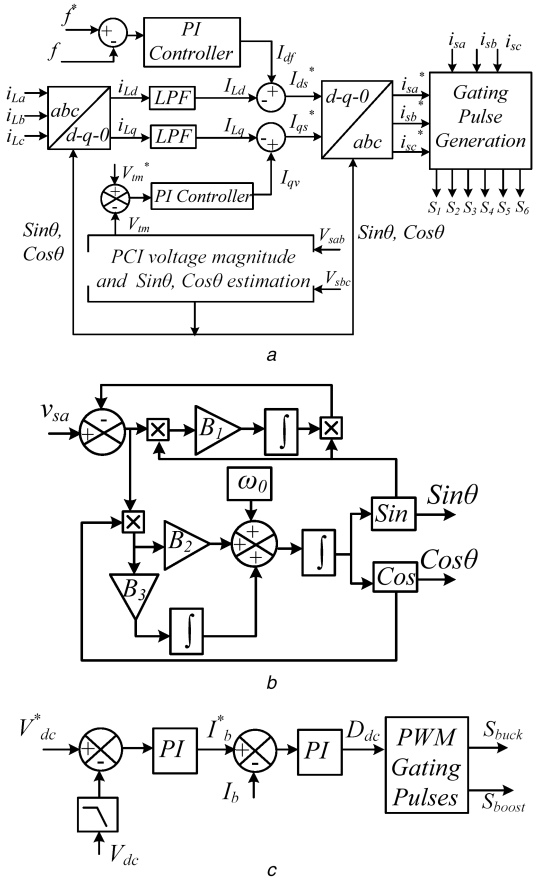

Fig. 2 *Control diagram of standalone MG*
(a) Control algorithm for VSC, ***(b)*** Estimation of $\sin\theta$ and $\cos\theta$ components, ***(c)*** Controller for BDDC

$$\begin{aligned}
&\text{if } \frac{\Delta I_{\text{pv}}}{\Delta V_{\text{pv}}} > -\frac{I_{\text{pv}}}{V_{\text{pv}}}, \text{then } w(m) = w(m-1) + \Delta w,\\
&\text{if } \frac{\Delta I_{\text{pv}}}{\Delta V_{\text{pv}}} = -\frac{I_{\text{pv}}}{V_{\text{pv}}}, \text{then } w(m) = w(m-1),\\
&\text{if } \frac{\Delta I_{\text{pv}}}{\Delta V_{\text{pv}}} < -\frac{I_{\text{pv}}}{V_{\text{pv}}}, \text{then } w(m) = w(m-1) - \Delta w,
\end{aligned} \tag{8}$$

where I_{pv} and V_{pv} are the sampled PV current and PV voltage of the array, $w(m)$, $w(m-1)$ and Δw are the estimated, old and change in the duty ratio.

3.2 Control strategy for VSC

The VSC control is based on an indirect current control algorithm in which VSC switching is based on reference source currents (i_{sa}*, i_{sb}*, i_{sc}*) as shown in Fig. 2*a*. This control algorithm is subdivided into several parts like estimation of the angle between fixed and rotating frames, estimation of real and reactive components of load currents, determination of reference source currents and switching of VSC.

3.2.1 Estimation of angle between fixed and rotating frame: The estimation of the angle between rotating (abc) and fixed frame (*dq*) is shown in Fig. 2*a*. In VSC, *dq* axis voltage values are aligned with PCI voltages. Therefore, the phase voltages of PCI, are used to estimate the transformation angle through an enhanced phase locked loop (EPLL). Using this transformation angle, enhanced phase locked loop (EPLL) also estimates the phase and frequency of the voltage. Unlike SRF, EPLL does not have closed loop control for estimation of the frequency and phase of the input signal. Therefore, EPLL reduces the computational burden of DSP (dSPACE-1103) and the dynamic response is fast for estimation of phase and frequency. The schematic diagram of EPLL is shown in Fig. 2*b*. The EPLL constants, B_1, B_2, and B_3, are selected as per the procedure given in [27].

3.2.2 Estimation of real component of reference source currents: The real component of reference source currents is equal to the difference of the real component of load currents and active component for regulation of frequency. The real component of the load current is determined through *d–q* transformation as follows:

$$\begin{aligned}
i_{\text{L}d} &= \left(\frac{2}{3}\right)\left(\sin(\theta)i_{\text{La}} + \sin\left(\theta - \frac{2\pi}{3}\right)i_{\text{Lb}} + \sin\left(\theta + \frac{2\pi}{3}\right)i_{\text{Lc}}\right),\\
i_{\text{L}q} &= \left(\frac{2}{3}\right)\left(\cos(\theta)i_{\text{La}} + \cos\left(\theta - \frac{2\pi}{3}\right)i_{\text{Lb}} + \cos\left(\theta + \frac{2\pi}{3}\right)i_{\text{Lc}}\right),
\end{aligned} \tag{9}$$

where i_{La}, i_{Lb}, and i_{Lc} are load currents, which are sensed through the Hall-effect current sensors and $\cos(\theta)$ and $\sin(\theta)$ are calculated using EPLL. The DC value of the active load current is achieved after low pass filter as shown in Fig. 2*a*.

The total real component of reference source current (I_{ds}*) is determined as

$$I^*_{\text{ds}} = I_{\text{df}} - I_{\text{L}d}, \tag{10}$$

where I_{df} is the current required for maintaining the frequency of the MG and it is estimated as

$$I_{\text{df}}(r) = I_{\text{df}}(r-1) + k_{\text{pf}}\{f_{\text{er}}(r) - f_{\text{er}}(r-1)\} + k_{\text{if}}f_{\text{er}}(r), \tag{11}$$

where f_{er} is the error between reference frequency (50 Hz) and calculated frequency of voltage, which is estimated through EPLL.

3.2.3 Estimation of reactive component of reference source currents: The reactive component of source current is the difference of $I_{\text{L}q}$ and the reactive part for regulation of PCI voltage (I_{qv}).The reactive part of load current ($i_{\text{L}q}$) is estimated through *d–q* transformation and it is given by (9). The total reactive portion of reference current is estimated as

$$I^*_{\text{qs}} = I_{\text{qv}} - I_{\text{L}q}, \tag{12}$$

where $I_{\text{L}q}$ is the reactive portion of the load currents, which is the resultant of low pass filter as shown in Fig. 2*a*.

I_{qv} is the reactive component for regulating the PCI voltage and it is estimated as

$$I_{\text{qv}}(r) = I_{\text{qv}}(r-1) + K_{\text{pa}}\{V_{\text{er}}(r) - V_{\text{er}}(r-1)\} + k_{\text{ia}}V_{\text{er}}(r), \tag{13}$$

where V_{er} is the error between reference PCI amplitude (V_{tm}*) (187.3V) and estimated PCI amplitude voltage (V_{tm}) and it is given as

$$V_{\text{er}} = V^*_{\text{tm}} - V_{\text{tm}}. \tag{14}$$

The PCI amplitude voltage is estimated as

$$V_{\text{tm}} = \sqrt{\left(\frac{2}{3}\right)} \times \sqrt{(v^2_{\text{sa}} + v^2_{\text{sb}} + v^2_{\text{sc}})}, \tag{15}$$

where v_{sa}, v_{sb}, and v_{sc} are phase voltages and these phase voltages are estimated from the PCI line voltages v_{sab} and v_{sbc} by using following equations:

$$\begin{aligned}
&v_{\text{sa}} = \frac{1}{3}(2v_{\text{sab}} + v_{\text{sbc}}), \quad v_{\text{sb}} = \frac{1}{3}(-v_{\text{sab}} + v_{\text{sbc}}),\\
&v_{\text{sc}} = \frac{1}{3}(-v_{\text{sab}} - 2v_{\text{sbc}}).
\end{aligned} \tag{16}$$

3.2.4 Estimation of reference source currents and VSC switching: The reference source currents (i_{sa}*, i_{sb}*, i_{sc}*) are

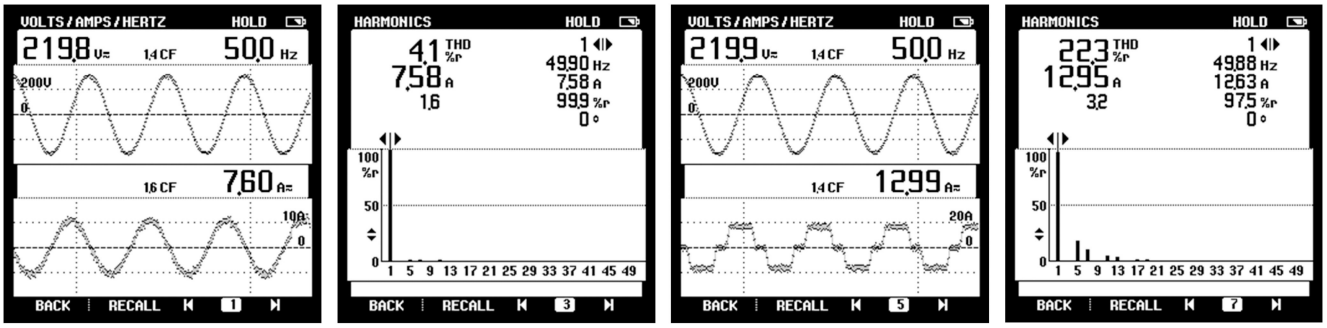

a *b* *c* *d*

Fig. 3 *Steady-state performance of PV-battery-hydro system under non-linear load*
(a) PCI line voltage (v_{sab}) and source current of phase 'c' (i_{sc}), ***(b)*** Harmonic spectra of i_{sa}, ***(c)*** v_{sab} and $i_{Lc}v_{sab}$ *and* i_{vscc}, ***(d)*** Harmonic spectra of $i_{Lc}p_s$

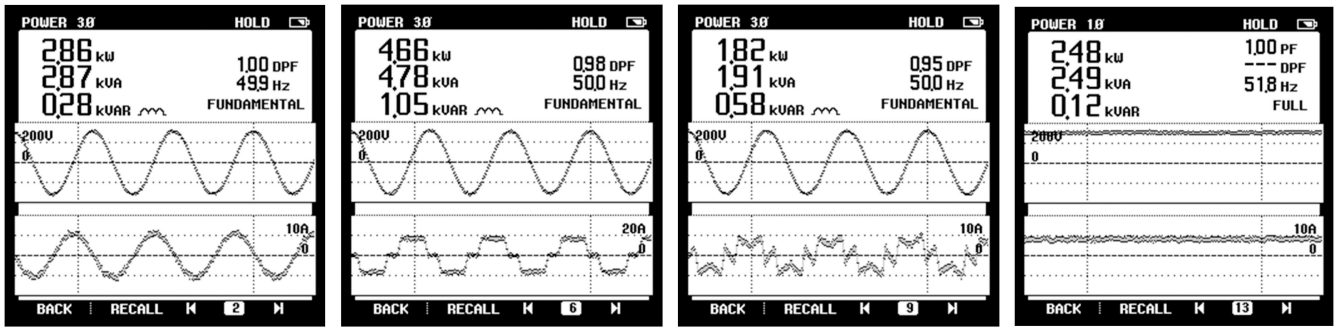

a *b* *c* *d*

Fig. 4 *Steady-state performance of PV-battery-hydro system under non-linear load*
(a) p_S, ***(b)*** p_L, ***(c)*** p_{vscc}, ***(d)*** P_{pv}

estimated by transforming the I_{ds}* and I_{qs}* into the three-phase quantity given as

$$\begin{aligned} i_{sa}^* &= \left(\sin(\theta)I_{ds}^* + \cos(\theta)I_{qs}^*\right), \\ i_{sb}^* &= \left(\sin\left(\theta - \frac{2\pi}{3}\right)I_{ds}^* + \cos\left(\theta - \frac{2\pi}{3}\right)I_{qs}^*\right), \\ i_{sc}^* &= \left(\sin\left(\theta + \frac{2\pi}{3}\right)I_{ds}^* + \cos\left(\theta + \frac{2\pi}{3}\right)I_{qs}^*\right). \end{aligned} \tag{17}$$

The hysteresis current controller generates the switching pulses for the VSC using the error of i_{sa}*, i_{sb}*, i_{sc}* and i_{sa}, i_{sb}, i_{sc}. The current errors (i_{sera}, i_{serb}, i_{serc}), are given as

$$i_{sera} = i_{sa}^* - i_{sa}, \quad i_{serb} = i_{sb}^* - i_{sb}, \quad i_{serc} = i_{sc}^* - i_{sc}. \tag{18}$$

3.3 Control strategy for BDDC

The control of the BDDC is shown in Fig. 2*c*. The BDDC regulates the DC bus voltage of the VSC while performing buck or boost operation depending on the battery charging or discharging. Moreover, the control synchronises the power generation and load demand by storing the surplus power into the battery. Similarly, the deficit power is supplied by the battery in case the generation is less than the load demand. The DC bus voltage is maintained by a proportional integral (PI) controller, which is expressed as

$$I_b^*(k) = I_b^*(k-1) + k_{pvi}\{V_{dcer}(k) - V_{dcer}(k-1)\} + k_{pvp}V_{dcer}, \tag{19}$$

where k_{pvi} and k_{pvp} are the gains of the PI controller, respectively

$$V_{dcer}(k) = V_{dc}^*(k-1) - V_{dc}(k). \tag{20}$$

The duty cycle of the converter is governed by a battery current PI controller and it is estimated as

$$D_{dc}(k) = D_{dc}(k-1) + k_{pii}\{I_{ber}(k) - I_{ber}(k-1)\} + k_{pip}I_{ber}, \tag{21}$$

where k_{pii} and k_{pip} are the gains of the PI controller, respectively

$$I_{ber}(k) = I_b^*(k-1) - I_b(k). \tag{22}$$

The pulse width modulation (PWM) pulses of the converter are achieved by comparison of the duty cycle with a saw-tooth signal.

4 Results and discussion

The proposed MG is implemented for a 3.7 kW hydro based induction generator, PV array simulator and BES. The performance of the proposed system is shown in Figs. 3–8 in a real-time experimental environment. The excitation capacitor of the SEIG has been selected by using the per-phase equivalent model of SEIG as per the procedure given in [28]. The per phase excitation capacitor of 3.7 kW, 230 V, 50 Hz, induction machine is selected as 80 µF/phase. Moreover, these capacitors are connected in delta configuration and it is connected to the generator terminals to maintain the rated voltage. A variable frequency drive controlled induction motor is used for emulating the hydro prime mover. A non-linear load is realised by using the diode bridge rectifier with the R–L load. Six Hall-effect current sensors are used for sensing the source currents (i_{sa} and i_{sb}), load currents (i_{La} and i_{Lb}), solar PV current (I_{pv}) and battery current (I_b). Four Hall-Effect voltage sensors are used for sensing the common point voltages (v_{sab} and v_{sbc}), PV voltage (V_{pv}) and the DC bus voltage of the converter (V_{dc}). A PV array simulator (TerraSAS PV) is used to realise a 2.48 kW solar PV, whose maximum voltage (V_{mpp}) and current (I_{mpp}) rating are 307.0 V and 8.0 A, respectively. The control algorithm of the VSC and a bidirectional converter for voltage, frequency and power management, are implemented on a digital controller (dSPACE-1103). The system voltage and frequency regulation are achieved by PI controllers. The PI controllers of the proposed MG are tuned using the Ziegler Nichols step response technique [29]. The detailed values of system parameters are given in the Appendix.

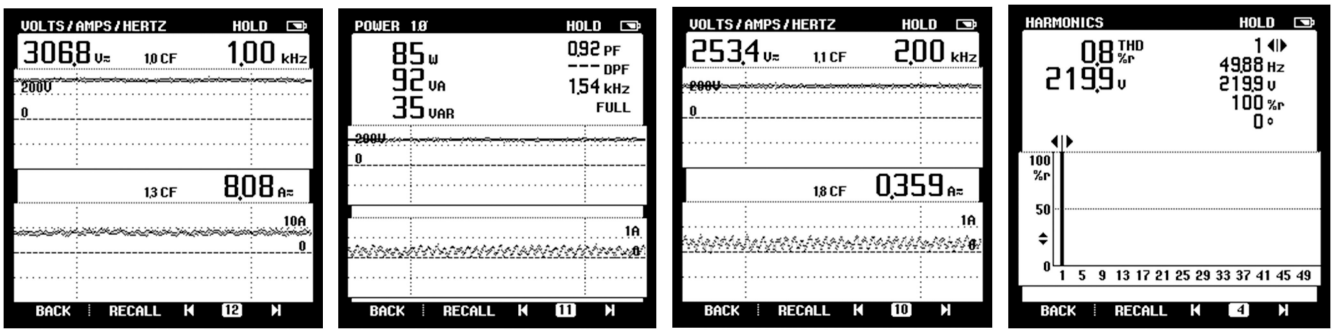

Fig. 5 *Steady-state performance of PV-battery-hydro system under non-linear load*
(a) V_{pv} and I_{pv}, ***(b)*** P_b, ***(c)*** V_b and I_b, ***(d)*** Harmonic spectra of v_{sab}

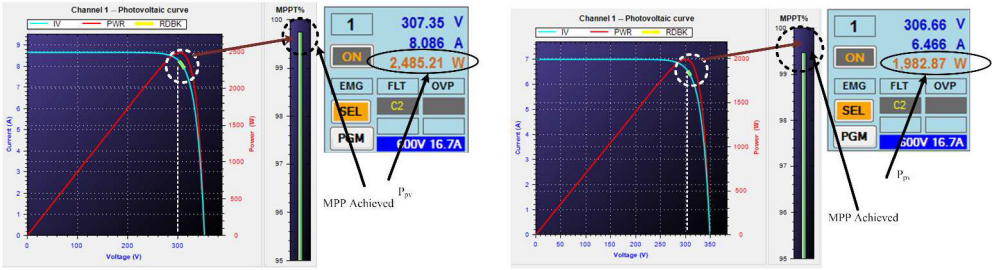

Fig. 6 *MPPT performance*
(a) at 1000 W/m^2, ***(b)*** at 790 W/m^2

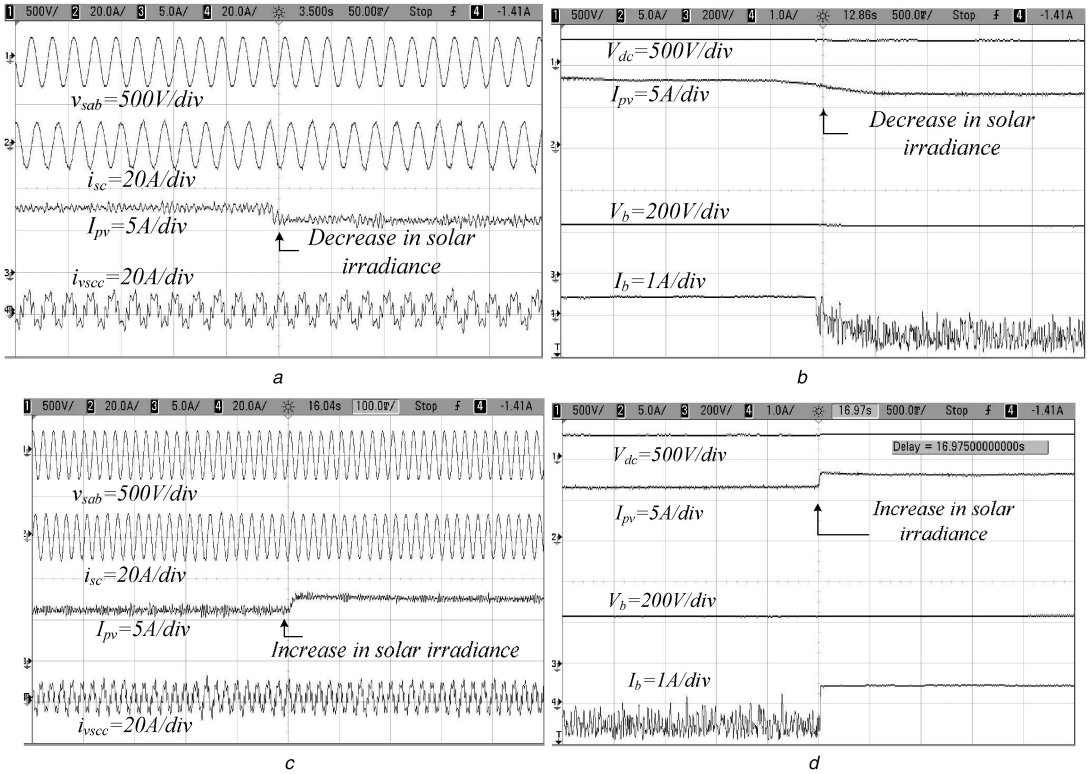

Fig. 7 *Dynamic performance of PV-battery-hydro based MG following by solar irradiance change*
(a) v_{sab}, i_{sc}, i_{Lc} and i_{vscc}, ***(b)*** V_{dc}, I_{pv}, V_b and I_b, ***(c)*** v_{sab}, i_{sa}, i_{La} and i_{vsca}, ***(d)*** V_{dc}, I_{pv}, V_b and I_b

4.1 Steady-state performance of PV-battery-hydro based MG under non-linear load

The current drawn by the non-linear load contains the harmonics and in the proposed MG, the hydro generated source currents are sinusoidal even when the load currents are non-sinusoidal as shown in Figs. 3*a–d*. The load is fed through two energy sources, one is hydro and second is PV array as shown in Figs. 4*a–d*. In the proposed MG, the MPPT algorithm harnesses the maximum available power from the solar PV array and the performance of the MPPT algorithm of the solar PV array simulator in the experimental prototype is shown in Fig. 6*a*. Solar PV generated power, voltage, and current under maximum power condition and also battery voltage, current and power are shown in Fig. 4*d* and 5*a–c*. From Fig. 4*d*, it is seen that the solar PV generated power is 2.48 kW, which is distributed into three parts (i) supplying the remaining power required by the load, (ii) storing the surplus

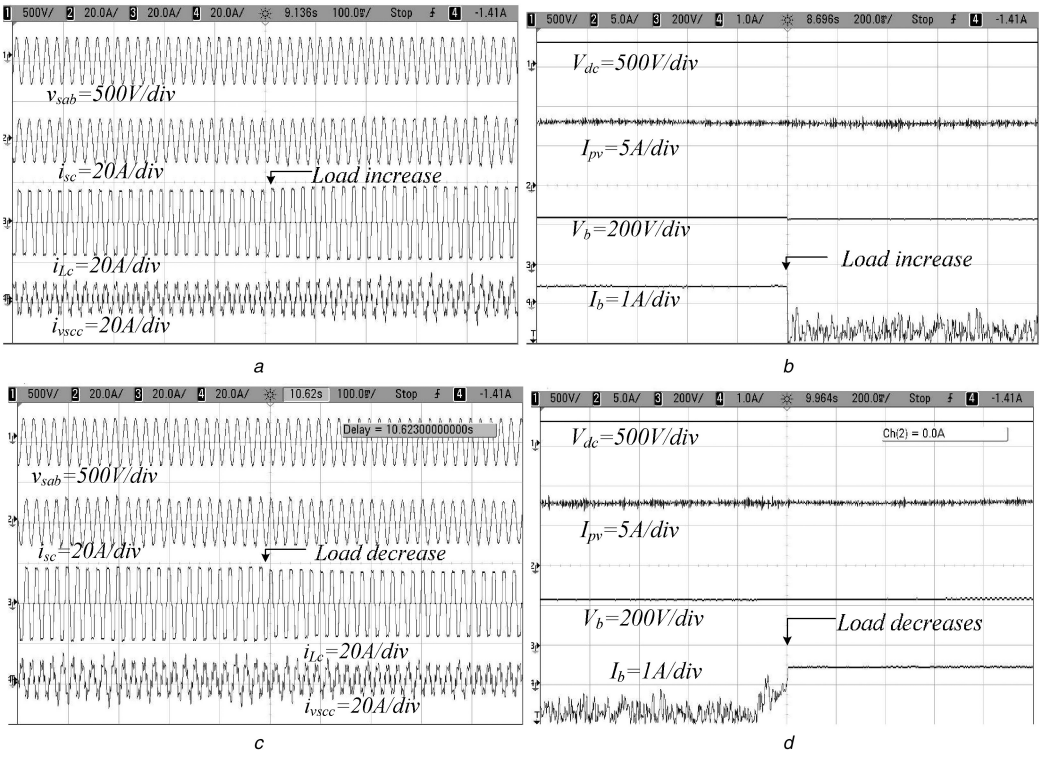

Fig. 8 *Dynamic performance of hydro-battery-PV based MG under load perturbation*
(a) v_{sab}, i_{sc}, I_{pv} and i_{vscc}, ***(b)*** V_{dc}, I_{pv}, V_b and I_b, **(c)** v_{sab}, i_{sc}, I_{pv} and i_{vscc}, ***(d)*** V_{dc}, I_{pv}, and V_b

power in the battery, and (iii) compensating losses of the system. The harmonic spectra of PCI line voltages, source current and load current, are shown in Figs. 3*b*, *d,* and 5*d*. The source current is sinusoidal and its total harmonic distortion (THD) is 4.1% and source voltage THD is 0.8%, which are well within an IEEE-519 standard. However, the load current THD is obtained as 22.3%.

4.2 Dynamic performance of PV-battery-hydro based MG under change in solar irradiance

The dynamic performance of the PV-battery-hydro based MG under solar irradiance disturbance is shown in Figs. 7*a–d* and 6*b*. In Figs. 7*a–d*, the dynamic behaviour of the PCI voltage (v_{sab}), source current (i_{sc}), load current (i_{Lc}), VSC current (i_{vscc}), DC-link voltage (V_{dc}), solar PV array current (I_{pv}), battery voltage (V_b) and battery current (I_b), is exhibited. Despite the change in solar PV irradiance from 1000 to 790 W/m^2, MPP is achieved as shown in Fig. 6*b*. A reduction in solar PV irradiance, causes the change in solar generated power and consequently, the change in battery operating mode from charging to discharging mode, to meet the load demand as shown in Fig. 7*b*. The other system parameters remain unaffected and the system remains stable. Similarly, an increase in solar PV irradiance, increases the power generated by the solar PV array. To manage the increased power, the battery changes the operating from discharging to charging as shown in Figs. 7*c–d*. The DC-link voltage remains unaffected under the solar irradiance disturbances.

4.3 Dynamic performance of PV-battery-hydro based MG under load perturbation

Fig. 8 presents the dynamic performance of PV-battery-hydro based MG under varying load conditions. Figs. 8*a–d* show the transient behaviour of the PCI voltage (v_{sab}), source current (i_{sc}), load current (i_{Lc}), VSC current (i_{vscc}), DC-link (V_{dc}), solar array current (I_{pv}), battery voltage (V_b) and battery current (I_b). When the load is increased, load demand exceeds the hydro generated power, since SEIG operates in constant power mode. In this condition, the solar power is diverted to meet the load demand and the battery starts discharging as shown in Figs. 8*a* and *b*. Similar is the condition for a decrease in load demand and the battery comes into charging mode, which is depicted in Figs. 8*c* and *d*.

5 Conclusions

In the proposed MG, an integration of hydro with the battery, compensates the intermittent nature of PV array. The proposed system uses the hydro, solar PV and battery energy to feed the voltage (V_{dc}), solar array current (I_{pv}), battery voltage (V_b) and battery current (I_b). When the load is increased, the load demand exceeds the hydro generated power, since SEIG operates in constant power mode condition. This system has the capability to adjust the dynamical power sharing among the different RES depending on the availability of renewable energy and load demand. A bidirectional converter controller has been successful to maintain DC-link voltage and the battery charging and discharging currents. Experimental results have validated the design and control of the proposed system and the feasibility of it for rural area electrification.

6 References

[1] Ellabban, O., Abu-Rub, H., Blaabjerg, F.: 'Renewable energy resources: current status, future prospects and technology', *Renew. Sustain. Energy Rev.*, 2014, **39**, pp. 748–764

[2] Bull, S.R.: 'Renewable energy today and tomorrow', *Proc. IEEE*, 2001, **89**, (8), pp. 1216–1226

[3] Malik, S.M., Ai, X., Sun, Y., *et al.*: 'Voltage and frequency control strategies of hybrid AC/DC microgrid: a review', *IET Renew. Power Gener.*, 2017, **11**, (2), pp. 303–313

[4] Kusakana, K.: 'Optimal scheduled power flow for distributed photovoltaic/wind/diesel generators with battery storage system', *IET Renew. Power Gener.*, 2015, **9**, (8), pp. 916–924

[5] Askarzadeh, A.: 'Solution for sizing a PV/diesel HPGS for isolated sites', *IET Renew. Power Gener.*, 2017, **11**, (1), pp. 143–151

[6] Kant, K., Jain, C., Singh, B.: 'A hybrid diesel-wind-PV based energy generation system with brushless generators', *IEEE Trans. Ind. Inf.*, 2017, **99**, pp. 1–1

[7] John, T., Ping Lam, S.: 'Voltage and frequency control during microgrid islanding in a multi-area multi-microgrid system', *IET Gener. Transm. Distrib.*, 2017, **11**, (6), pp. 1502–1512

[8] Philip, J., Jain, C., Kant, K., *et al.*: 'Control and implementation of a standalone solar photo-voltaic hybrid system', *IEEE Trans. Ind. Appl.*, 2016, **52**, (4), pp. 3472–3479

[9] Kwon, M., Choi, S.: 'Control scheme for autonomous and seamless mode switching of bidirectional DC–DC converters in a DC microgrid', *IEEE Trans. Power Electron.*, 2017, early access
[10] Merabet, A., Tawfique Ahmed, K., Ibrahim, H., *et al.*: 'Energy management and control system for laboratory scale microgrid based wind-PV-battery', *IEEE Trans. Sustain. Energy*, 2017, **8**, (1), pp. 145–154
[11] Prakash, S.L., Arutchelvi, M., Jesudaiyan, A.S.: 'Autonomous PV-array excited wind-driven induction generator for off-grid application in India', *IEEE J. Emerg. Sel. Top. Power Electron.*, 2016, **4**, (4), pp. 1259–1269
[12] Atia, R., Yamada, N.: 'Sizing and analysis of renewable energy and battery systems in residential microgrids', *IEEE Trans. Smart Grid*, 2016, **7**, (3), pp. 1204–1213
[13] Sobhan, N.: 'Automatic generation control and monitoring the mechanism of micro hydro power plant with impulse turbine and synchronous generator'. *Proc. Int. Conf. on Robotics and Artificial Intelligence*, 2016, pp. 175–179
[14] Nicy, C.F., Punitharaji, R.: 'Isolated wind-hydro hybrid system using permanent magnet synchronous generator and battery storage with fuzzy logic controller'. Proc. Int. Conf. on Green Computing Communications and Electrical Engineering (ICGCCEE), 2014, pp. 1–6
[15] Rathore, U.C., Singh, S.: 'Power quality control of SEIG based isolated pico hydro power plant feeding non-linear load'. IEEE 6th India Int. Conf. on Power Electronics (IICPE), 2014, pp. 1–5
[16] Tamrakar, I., Shilpakar, L., Fernandes, B., *et al.*: 'Voltage and frequency control of parallel operated synchronous generator and induction generator with STATCOM in micro hydro scheme', *IET Gener. Transm. Distrib.*, 2007, **1**, (5), pp. 743–750
[17] Scherer, L.G., Tambara, R.V., de Camargo, R.F.: 'Voltage and frequency regulation of standalone self-excited induction generator for micro-hydro power generation using discrete-time adaptive control', *IET Renew. Power Gener.*, 2016, **10**, (4), pp. 531–540
[18] Chilipi, R.R., Singh, B., Murthy, S.S., *et al.*: 'Design and implementation of dynamic electronic load controller for three-phase self-excited induction generator in remote small-hydro power generation', *IET Renew. Power Gener.*, 2014, **8**, (3), pp. 269–280
[19] Singh, B., Murthy, S.S., Reddy, R.S., *et al.*: 'Implementation of modified current synchronous detection method for voltage control of self-excited induction generator', *IET Power Electron.*, 2015, **8**, (7), pp. 1146–1155
[20] Singh, B., Murthy, S.S., Gupta, S.: 'STATCOM-based voltage regulator for self-excited induction generator feeding nonlinear loads', *IEEE Trans. Ind. Electron.*, 2006, **53**, (5), pp. 1437–1452
[21] Singh, B., Kasal, G.K.: 'Voltage and frequency controller for a three-phase four-wire autonomous wind energy conversion system', *IEEE Trans. Energy Convers.*, 2008, **23**, (2), pp. 509–518
[22] Serban, I., Marinescu, C.: 'Control strategy of three-phase battery energy storage systems for frequency support in microgrids and with uninterrupted supply of local loads', *IEEE Trans. Power Electron.*, 2014, **29**, (9), pp. 5010–5020
[23] Eghtedarpour, N., Farjah, E.: 'Distributed charge/discharge control of energy storages in a renewable-energy-based DC micro-grid', *IET Renew. Power Gener.*, 2014, **8**, (1), pp. 45–57
[24] Arai, J., Iba, K., Funabashi, T., *et al.*: 'Power electronics and its applications to renewable energy in Japan'. *IEEE Circ. Syst. Mag.*, 2008, **8**, pp. 52–66
[25] Seema Singh, B.: 'Intelligent control of SPV-battery-Hydro based microgrid'. Proc. Power Electronics Drives Energy Systems (PEDES), 2016, pp. 1–6
[26] Elgendy, M., Zahawi, B., Atkinson, D.: 'Assessment of the incremental conductance MPPT algorithm', *IEEE Trans. Sustain. Energy*, 2013, **4**, (1), pp. 108–117
[27] Karimi-Ghartemani, M., Ooi, B.T., Bakhshai, A.: 'Application of enhanced phase-locked loop system to the computation of synchrophasors', *IEEE Trans. Power Deliv.*, 2011, **26**, (1), pp. 22–32
[28] Singh, B., Murthy, S.S., Gupta, S.: 'Analysis and design of electronic load controller for self-excited induction generators', *IEEE Trans. Energy Convers.*, 2006, **21**, (1), pp. 285–293
[29] Singh, B., Kasal, G.K.: 'Solid state voltage and frequency controller for a stand alone wind power generating system', *IEEE Trans. Power Electron.*, 2008, **23**, (3), pp. 1170–1177

7 Appendix

Parameters for proposed MG: 3.7 kW, 230 V, 50 Hz, star-connected and four-pole SEIG, $L_b = 6$ mH, $L_f = 5$ mH; battery capacity 240 V, 14 Ah, EPLL constant $B_1 = 0.1 \times 10^3$, $B_2 = 0.05 \times 10^2$ and $B_3 = 0.02 \times 10^3$; PCI voltage PI controller gain: $k_{pa} = 0.1$, $k_{ia} = 1.6$; $L_{dc} = 4$ mH, PI controller gain of DC–DC bidirectional controller: $k_{pvp} = 2$, $k_{pvi} = 0.0001$and $k_{pip} = 3$, $k_{pii} = 0.0001$; $P_{mpp} = 2.48$ kW, $V_{mpp} = 307.35$ V and $I_{mpp} = 8.086$ A.